Neuroscience Research 103 (2016) 10–17

Contents lists available at ScienceDirect

Neuroscience Research

journal homepage: www.elsevier.com/locate/neures

Ultrastructural analysis of olfactory ensheathing cells derived from olfactory bulb and nerve of neonatal and juvenile rats

Rosa M. Gómez[a,b,*], Kemel Ghotme[a,c], Lucía Botero[d], Jaime E. Bernal[e], Rosalía Pérez[a], George E. Barreto[f,g], Rosa Helena Bustos[a,h]

[a] Facultad de Medicina, Universidad de La Sabana, Campus Universitario Puente del Común, Km 7 Autopista Norte, Chía, Colombia
[b] Fundación Neuroregeneración de Colombia, Colombia
[c] Unidad de Neurocirugía, Fundación Santafé de Bogotá, Colombia
[d] Facultad de Medicina Veterinaria y Zootecnia, Universidad Nacional de Colombia, Colombia
[e] Instituto de Genetica, Universidad Javeriana, Carrera 7 No 45-02, Bogota, Colombia
[f] Departamento de Nutrición y Bioquímica, Facultad de Ciencias, Pontificia Universidad Javeriana, Bogotá D.C., Colombia
[g] Instituto de Ciencias Biomédicas, Universidad Autónoma de Chile, Santiago, Chile
[h] Grupo Evidencia Terapéutica, Departamento de Farmacología, Universidad de La Sabana, Colombia

ARTICLE INFO

Article history:
Received 26 March 2015
Received in revised form 24 July 2015
Accepted 29 July 2015
Available online 6 August 2015

Keywords:
Olfactory ensheathing cells
Electron microscopy
Regeneration
Neural repair
Cell therapy

ABSTRACT

Olfactory nerve derived and olfactory bulb derived olfactory ensheathing cells (OECs) have the ability to promote axonal regeneration and remyelination, both of which are essential in a successful cell transplant. Thus, morphological identification of OECs is a key aspect to develop an applicable cell therapy for injuries to the nervous system. However, there is no clear definition regarding which developmental stage or anatomical origin of OECs is more adequate for neural repair. In the present study, an ultrastructural comparison was made between OECs recovered from primary cultures of olfactory nerve and bulb in two developmental stages. The most notorious difference between cells obtained from olfactory nerve and bulb was the presence of indented nuclei in bulb derived OECs, suggesting a greater ability for possible chemotaxis. In neonatal OECs abundant mitochondria, lipid vacuoles, and smooth endoplasmic reticulum were detected, suggesting an active lipid metabolism, probably involved in synthesis of myelin. Our results suggest that neonatal OECs obtained from olfactory bulb have microscopic properties that could make them more suitable for neural repair.

© 2015 Elsevier Ireland Ltd and the Japan Neuroscience Society. All rights reserved.

1. Introduction

OECs are located in the Central Nervous System (CNS), distributed in the two outer layers of the olfactory bulb and in the peripheral nervous system, along the path of the olfactory pathway from olfactory mucosa to bulb and actively participate in growth and location of olfactory axons during development. OECs have the ability, as growth promoters (Pellitteri et al., 2007), to induce axonal regeneration and remyelination (Zhu et al., 2010) both of which are essential in a successful spinal cord transplant and consequently they have been proposed as candidates for regeneration in mammalian visual system (Plant et al., 2011) and transplantation following spinal cord injury (Chou et al., 2014; Franssen et al., 2007). Previous studies indicate three types of OECs: Olfactory Bulb (OB), Olfactory Nerve (ON), and Olfactory Lamina (OL) (Ozdemir et al., 2012; Roet and Verhaagen, 2014).

Some OECs within the olfactory pathway exhibit an elongated morphology and extend thin laminar processes that enfold olfactory nerves, while others have a rounded shape and may fail to enfold (Valverde et al., 1992). Different OECs morphologies, including flat, bipolar and tripolar shapes, have been identified in cultures from the olfactory epithelium, *lamina propria*, olfactory nerves, and outer olfactory bulb layer of embryonic, neonatal or adult rats and mice (Au and Roskams, 2003; van den Pol and Santarelli, 2003). They present characteristic indented nuclei with uniformly distributed, although slightly clumped chromatin, below the nuclear membrane, large inclusion bodies are abundant in the cytoplasm. Ensheathing glia progenitors can be clearly distinguished from other migrating cells by their dark appearance, mode of association with axons, and ultrastructural features; their scanty cytoplasm contains a typical lobulated electro-dense nucleus with patchy chromatin beneath the nuclear envelope and one or two nucleoli (Valverde et al., 1992).

* Corresponding author at: Universidad de la Sabana, Campus Universitario Puente del Común, Km 7 Autopista Norte, Chía, Colombia. Tel.: +57 8615555x27333.
E-mail address: rosa.gomez@unisabana.edu.co (R.M. Gómez).

http://dx.doi.org/10.1016/j.neures.2015.07.012
0168-0102/© 2015 Elsevier Ireland Ltd and the Japan Neuroscience Society. All rights reserved.

Microscopic morphological identification of OECs is a key aspect in order to design a therapeutic approach for CNS injuries. Morphological description of OECs cultures taken from different locations and at different ages can provide valuable information regarding which cell type is the most adequate for transplant in spinal cord injury models. However, there is not a clear definition regarding what developmental stage and what anatomical origin of OECs is more adequate for cell therapies. This study provides a morphological characterization of OECs by immunohistochemistry, transmission electron microscopy (TEM), and scanning electron microscopy (SEM) in two developmental stages (neonatal and juvenile) and two olfactory tissues (ON and OB).

2. Materials and methods

ON and OB tissues were obtained from Wistar specific pathogen free (SPF) rats: 20 juvenile rats (3–6 months of age) and 20 neonatal rats (5–10 days of age). All rats were euthanized under the 2013 AVMA Guidelines for the Euthanasia of Animal.

2.1. Primary cultures of OECs

After a careful dissection under a stereoscope, olfactory nerves and bulbs were obtained and the tissues were washed three times with Hank's 1× (Sigma) supplemented with penicillin 100 U/mL, streptomycin 100 mg/mL, and amphotericin B 0.25 μg/mL (Gibco). The tissues were subjected to enzymatic dissociation with collagenase 0.1% (Sigma–Aldrich) for 10 min at 37 °C and 5% CO_2, and the mixture was centrifuged at 330 g for 10 min; the cell pellet was re-suspended in Dulbecco's Modified Eagle Medium (DMEM) with 4.50 mg/L D-glucose with sodium pyruvate, phenol red, with 4.7 g/L sodium bicarbonate (Gibco), supplemented with fetal bovine serum 20% (Gibco) with penicillin 100 IU mL, streptomycin 100 mg/mL, and amphotericin B 0.25 mg/mL (Gibco). The cell suspension was then seeded in 6-well plates. After 18 h, the supernatant was seeded in 6-well plates for 36 h and finally this supernatant was seeded again in polyvinyl micro crop boxes and polycationic proteins, until obtaining a confluence of 80%. OECs obtained were seeded at a cell density of 4 × 105 cells/mL in Falcon 24-well plates in an area of 0.1 cm^2 on coverslips, previously treated with 0.01% collagen (Sigma) and poly-D-lysine (Sigma) plus Aclar Hats.

Cultures were monitored daily under inverted microscope (Nikon Eclipse TS100, Japan) (Richter et al., 2008). Subsequently, for the electron microscopy analysis, the OECs from both groups (neonatal and juvenile rats) were fixed and processed in 2% glutaraldehyde (Sigma), and then processed with osmium tetroxide (02595-BASPI-Chem™) and gold-palladium (LM/EM Silver Enhancement Kit 04180-AB).

2.2. Immunohistochemistry

Primary antibodies were utilized for detection of protein S-100β (calcium-binding protein) (Sigma), glial fibrillary acidic protein (GFAP) (Sigma) and $p75^{NTR}$ (neurotrophin receptor) (Sigma), and cells were incubated for 1 h at 37 °C. The primary antibodies used were: mouse monoclonal 1:75 in 0.1 M PBS for detecting $p75^{NTR}$ IgG1 (Sigma); mouse monoclonal specific IgG to S-100β 1:500 in 0.1 M PBS (Sigma and Dako, respectively); and rabbit polyclonal IgG to detect GFAP 1:1 in 0.1 M PBS (Sigma). Finally, specific secondary antibodies were used for all immunosections. The number of OECs expressing antibodies S-100β, GFAP and $p75^{NTR}$ in light microscopy were counted, 1000 and 500 cells per field for a total of 360 samples, by using a Nikon Eclipse TS100 and Olympus CX 21.

2.3. Transmission electron microscopy (TEM)

TEM was performed on a Hitachi HU-12A. Cells were fixed with 2% glutaraldehyde (Sigma) for 1 h at room temperature. Three washes were made with PBS (Sigma) for 10 min each and then were fixed with osmium tetroxide (02595 – BASPI-Chem™). Cells were dehydrated for 20 min with serial changes in absolute ethanol (Merck) at 70%, 80%, 85%, 90%, 95%, and 100%. Once dehydrated, cells were subjected to inclusion in EPON® Resin (Merck) with serial combined changes with resin/propylene oxide (SPI-Chem™) and finally polymerized at 60 °C. Cells were observed after ultra-thin sections. For the TEM analysis, the electrodense chromogen diaminobenzidine was used at 0.1% (Sigma), to show whether or not the cells were expressing the above-mentioned proteins.

2.4. Scanning electron microscopy (SEM)

Cells were fixed with 2% glutaraldehyde for 1 h at room temperature. Three washings were made with PBS (Sigma) for 10 min each, and then dehydrated for 10 min with serial changes in absolute ethanol (Merck) at 70%, 80%, 85%, 90%, 95%, and 100%. Once dehydrated, cells were metallized with Palladium (Gold-Palladium LM/EM-04180 Silver Enhancement Kit AB). SEM was carried out on a Bal-Tec Sputter Coater 0.50 Fei Quanta 200.

3. Results

Primary cultures of OECs were obtained from olfactory nerve and olfactory bulb from 10-day-old neonatal and 3 month-old juvenile rats (Fig. 1). Cultures were maintained until confluence was reached, and we achieved isolation of approximately 80% OECs from the OB and ON using a technique as previously described (Nash et al., 2001). Subsequently OECs were fixed and processed for immunocytochemistry and electron microscopy.

In this first observation, cells were spindle-shaped like with large cytoplasm, with a tendency to have a patchy growth pattern with a thick internal membrane. Some areas of cellular growth, a property of cells with mitogenesis, are also noted (Fig. 1A and B), suggesting a possible capacity of OECs for proliferation. Addition of serum to the OEG containing cultures increased the number of BIII-tubulin positive neurites growing out of the explants and extending for short distances compared with OEG treatments lacking serum (Leaver et al., 2006). From this first characterization, it can be assumed that there are no significant morphological differences between ON and OB-derived cells in terms of culture pattern (Fig. 1C and D).

3.1. Immunocytochemistry

To better characterize the markers expressed by both cell types, we stained cells for S100β and GFAP markers in OB and ON-derived OECs of neonatal and juvenile Wistar rats. We observed that OECs are immunoreactive for S100β and GFAP and their shape varied from bipolar spindly to stellate (Fig. 2). Cells with a morphology similar to astrocytes represent a small percentage of the total GFAP positive cells, as previously reported (Barber and Lindsay, 1982; Pixley, 1992). Their presence is significantly reduced in the cultures, suggesting that these cells identified as OECs with similar morphology to astrocytes might actually be astrocytes. However, the morphology appears to vary depending on the site of collection of the cells and their state of development. OECs, in this study, were also positive for p75 NTR (Fig. 3).

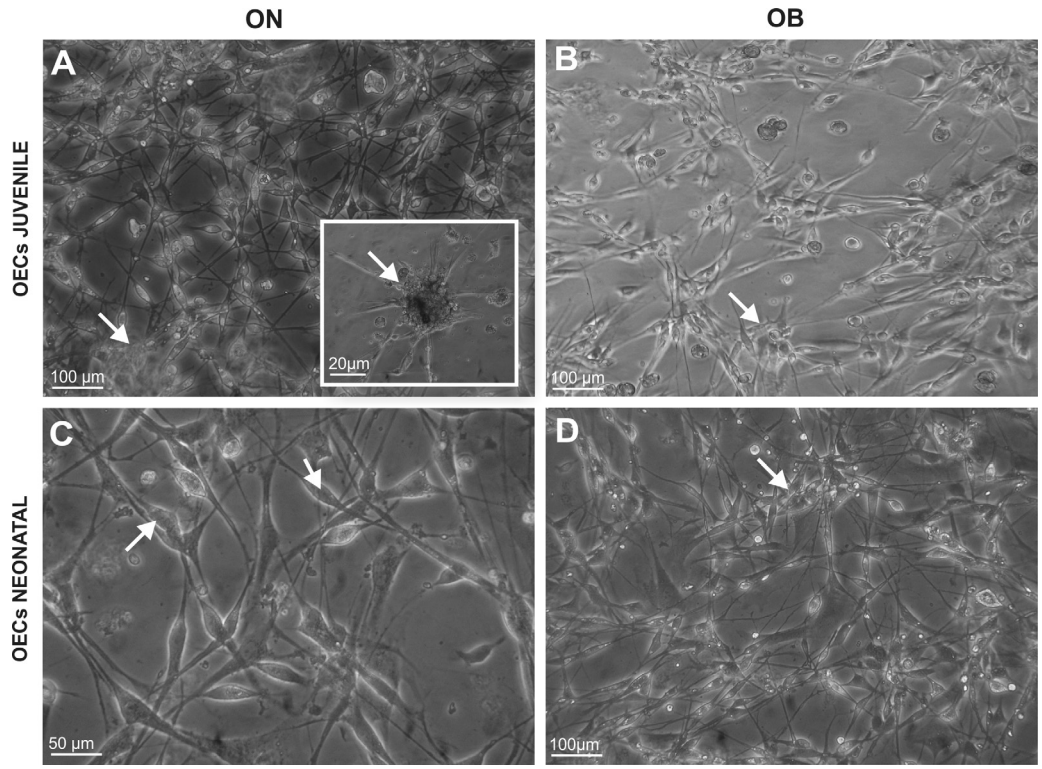


Fig. 1. OECs primary cultures, juvenile rat. (A) OECs sphere growth. (B) OECs patchy growth (arrows) and sparse growth (arrowheads). (C) ON-derived OECs. (D) OB-derived OECs.

3.2. Transmission electron microscopy (TEM)

3.2.1. Juvenile OECs

TEM studies were performed on OECs positively marked for S100β and GFAP. In general, juvenile cells were irregularly shaped and their size ranged from 5 to 20 μm (Fig. 4). ON-derived cells showed a typical flat appearance with cytoplasmic projections, similar to astrocyte cells, and nuclei localized toward one of the ends with a ratio with the cytoplasm of 2.5:1, and the cell membrane appeare ruffled. The cellular content was electro lucid with fiber-shaped structures. The nuclei were round or elongated without indentations, with peripheral aggregates of heterochromatin (Fig. 4A–F).

OB-derived cells showed a spindle-shaped configuration with large nuclei and cytoplasm with electro dense vacuoles and granules (Fig. 4D–F). The nuclei were rounded and indented with a nucleus–cytoplasm ratio of 2:1 and with aggregates of heterochromatin at the periphery (more evident than in the nerve cells). The average culture size was 10 microns. In neither of the two origins (i.e., OB or ON), cells showed endoplasmic reticulum. A significant proportion of large sized vesicles with fragmented and diffuse content, consistent with phagolysosomes, were observed.

3.2.2. Neonatal OECs

Presence of mitochondria was more prominent in neonatal than in juvenile cultures. Also, cells showed multiple vesicular structures accumulating lipids and lipoproteins accompanied by abundant mitochondria, characteristic of ensheathing glial cells. In addition, they had abundant smooth endoplasmic reticulum (Fig. 5A–F).

ON-derived OECs showed similar features to juvenile OECs but with more prominent projections and a nucleus-cytoplasm ratio of 1.5:1 (Fig. 5A–C) s. Nuclei were also rounded or elongated, non-indented and also with peripheral aggregates of heterochromatin. In some neonatal cells a rough endoplasmic reticulum and some mitochondria were also observed.

OB-derived cells in neonates have similar characteristics than the ones previously described for juvenile rats but with a more prominent vacuole configuration. Nuclei were also rounded but, in this case, indented. Large size vesicles with fragmented and diffuse content, consistent with phagolysosomes were also observed, but in less proportion than in juvenile cells (Fig. 5D–F). Our results show that these cells type cultured from juvenile rat OB are capable of enfolding olfactory axons in vitro (Fig. 5G).

3.3. Scanning electron microscopy (SEM)

It is possible to identify ON-derived neonatal and juvenile OECs with similar morphology to Schwann cells, i.e., spindle-shaped (elongated, bipolar; Fig. 6). There were no significant differences between neonatal and juvenile cells or between OB and ON-derived cells in terms of morphology in SEM. The ultrastructure properties of the OEC characteristics for the two subtypes and developmental stages observed in our study are summarized in Table 1.

4. Discussion

Microscopic morphological characterization of OECs can help researchers in determining its properties by demonstrating differences between tissues and stages of development, which might be applicable for their use in axonal regeneration. Microscopic studies of cultured OECs have shown morphologic differences among cultures obtained from *lamina propria* of nasal mucosa and from olfactory bulb (Kueh et al., 2011; Watanabe et al., 2006). However, there is little evidence regarding morphological ultrastructure particularities in different developmental stages and in different anatomical origins of OECs, including olfactory nerve. In this study, we assessed a thorough ultrastructure description of OECs obtained

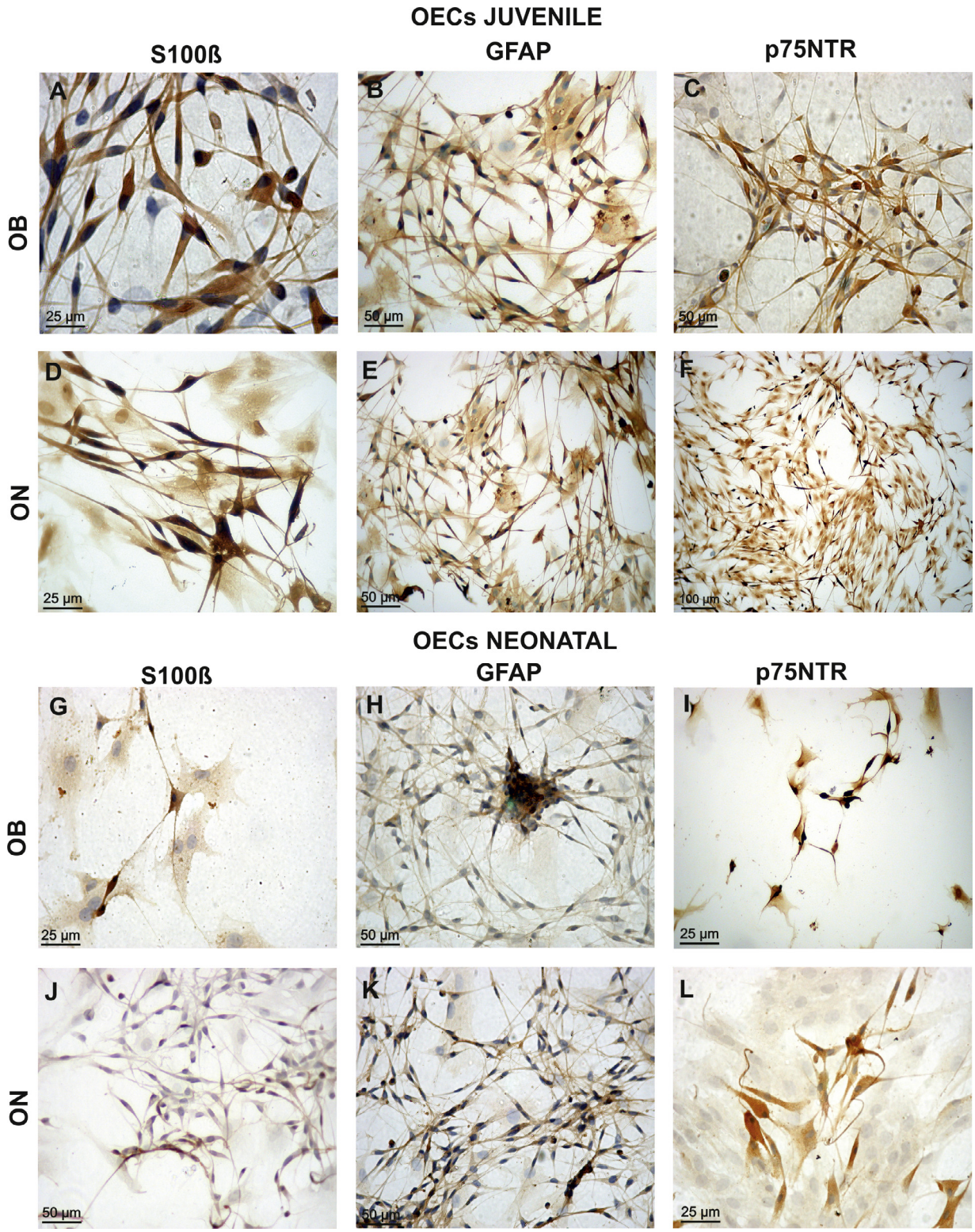


Fig. 2. Immunohistochemical microphotograph of OECs. (A) OB-derived OECs of juvenile rat, marking expressing S100β, GFAP and P75NTR. (B) ON-derived OECs of juvenile rat, marking expressing S100β, GFAP and P75NTR. (C) OB-derived OECs of neonatal rat labeled with S100β, GFAP and P75NTR. (D) ON-derived OECs of neonatal rat labeled with S100β, GFAP and P75NTR.

from olfactory bulb and olfactory nerve in neonatal and juvenile stages of development. In general, OECs in this study showed elongated cell shape with elongated nuclei with peripheral condensed chromatin. Some studies have suggested two distinct morphological patterns in the cells identified in cultures as OECs: (1) OECs with similar morphology to Schwann cells, i.e., spindle-shaped (elongated – bipolar), positive for S100β and GFAP (the latter generally has a weak expression) and (2) OECs with astrocyte-like morphology, which display varying flattened shapes (multipolar), but that are positive for GFAP (strong staining pattern with defined

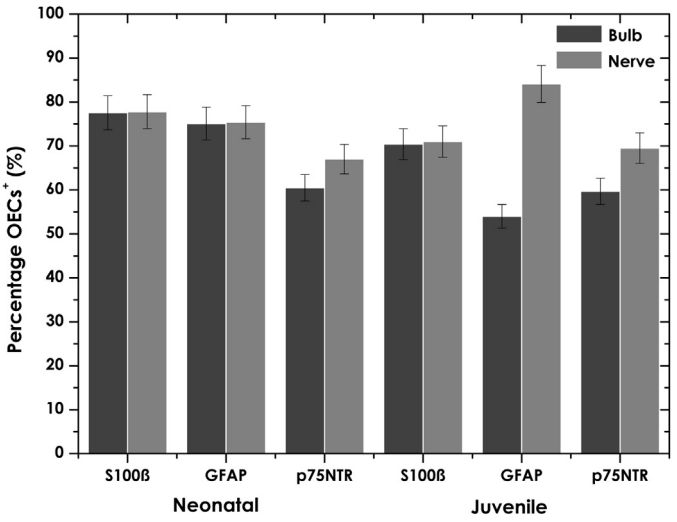


Fig. 3. Number of immunoreactive cells for S100β, GFAP and P75NTR. OECs were obtained either from OB or ON from juvenile and neonatal rats. During the development of rats and among nerve tissues, we observed that no juvenile rats had a higher percentage of CGEO cells (about 41.5%) in comparison to OB (22.7% in juvenile and 35.2% in neonatal).

filaments) and earn the S100β expression in culture (Goodman et al., 1993; Higginson and Barnett, 2011; Ramon-Cueto and Nieto-Sampedro, 1992). The two cell types described above were not observed in this study but elongated Schwann-like cells were identified. This difference could be due to the utilization of diverse culture techniques (Higginson and Barnett, 2011).

In this study, the most notorious difference between cells obtained from OB and ON was the presence of indented nuclei in OB-derived OECs. Previous indicated reported that OB-derived $p75^{NTR}$ immunoreactive cells exhibited lobulated nuclei with deep invaginations located in the center of the cell (Ramon-Cueto et al., 1993; Wewetzer et al., 2005). Recent studies about the genome wide transcriptional profiling and proteomic analysis have provided novel insights the OECs with their pro regenerative properties (Roet and Verhaagen, 2014). These cells present several genes with well-defined roles in cytoskeletal organization of process formation and cell motility, including MAP1B, MAP2, NEFL and APP (Ozdemir et al., 2012; Roet and Verhaagen, 2014). This emphasizes the importance for neural repair. Now the function attributed to these lobulations in OB-OECs. It has been suggested that the lobulations can be related to a regulatory function increased fluidity that may facilitate chemotaxis (Hoffmann et al., 2007). Of particular interest are also distributed chromatin Ramón-Cueto et al. (Ramon-Cueto et al., 1993) reported uniformly, with slight dense patches just below the nuclear membrane, similar to what was observed in this study.

Important differences were also observed between developmental stages. For example, in neonatal OECs, abundant mitochondria were observed as well as vacuoles filled with lipid content. Smooth endoplasmic reticulum was also seen with evident relation to the abovementioned vacuoles. These findings suggest an active lipid metabolism in neonatal OECs, probably involved in synthesis of myelin. Previous studies showed that fetal OECs are able to synthetize myelin as well as Schwann cells (Devon and Doucette, 1995; Doucette, 1984; Sasaki et al., 2007, 2011). Primary cultures of OECs have the ability to express CNPase, a marker of myelin forming cells present in cell membrane and microtubules, indicating that OECs have an intrinsic machinery to produce myelin (Radtke et al., 2011). Moreover, OECs' ability to produce myelin has also been shown in vivo (Boyd et al., 2005; Sasaki et al., 2011) and in models of demyelination in spinal cord (Kocsis et al., 2009). Also, important is the presence of $p75^{NTR}$ expressed by neonatal OECs in this study (Fig. 3), thus suggesting myelin formation activity, and this observation is in accordance with previous studies (Coutts et al., 2013; Kumar et al., 2005; Pellitteri et al., 2010). Altogether, these

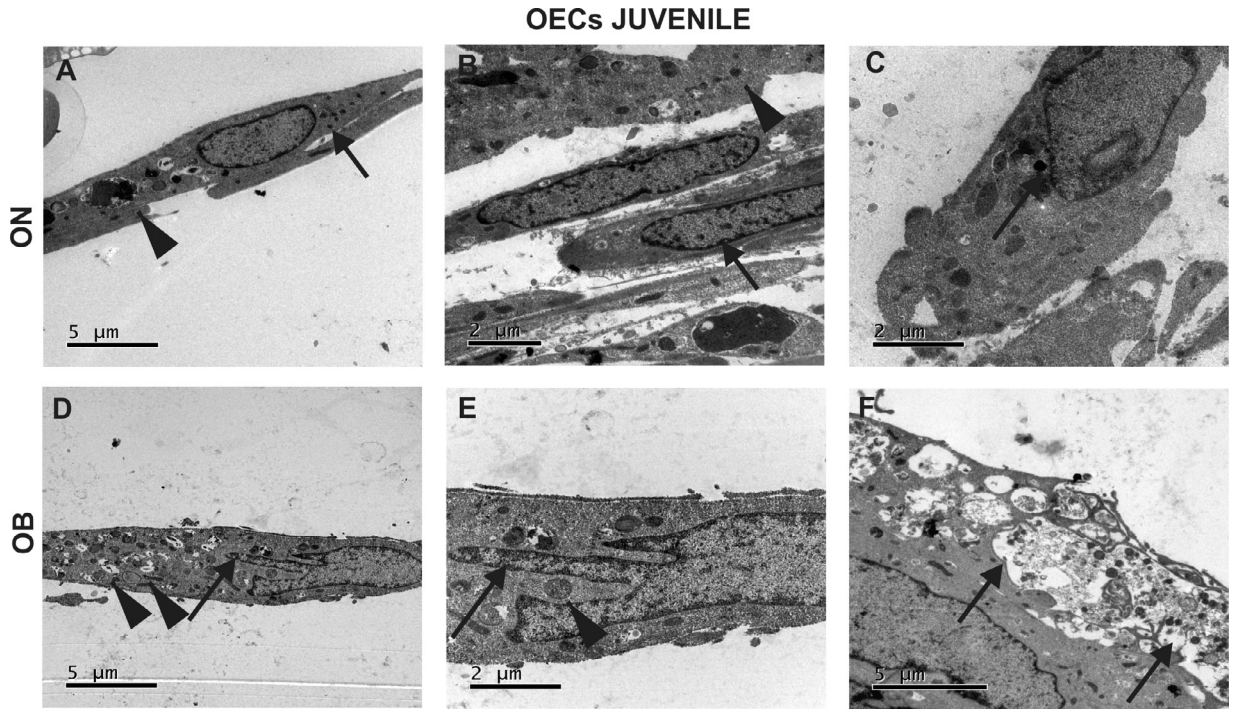


Fig. 4. Microphotograph of juvenile OECs by TEM labeled with S100β and GFAP. (A–C): Juvenile ON-derived OECs. (A) Elongated cells with extended nuclei displaced to one side of the cell body, some mitochondria (arrow) and lysosomes with content (arrowheads). (B) Elongated no indented nuclei (arrows) and few mitochondria (arrowheads). (C) Endoplasmic reticulum is not evident. (D–F): Juvenile OB-derived cells. (D) Elongated indented nuclei (arrowhead), large vesicles with abundant fragmented content (arrows). (E) Non-indented nuclei (arrows) and few mitochondria. (F) Lysosomes content (arrows).

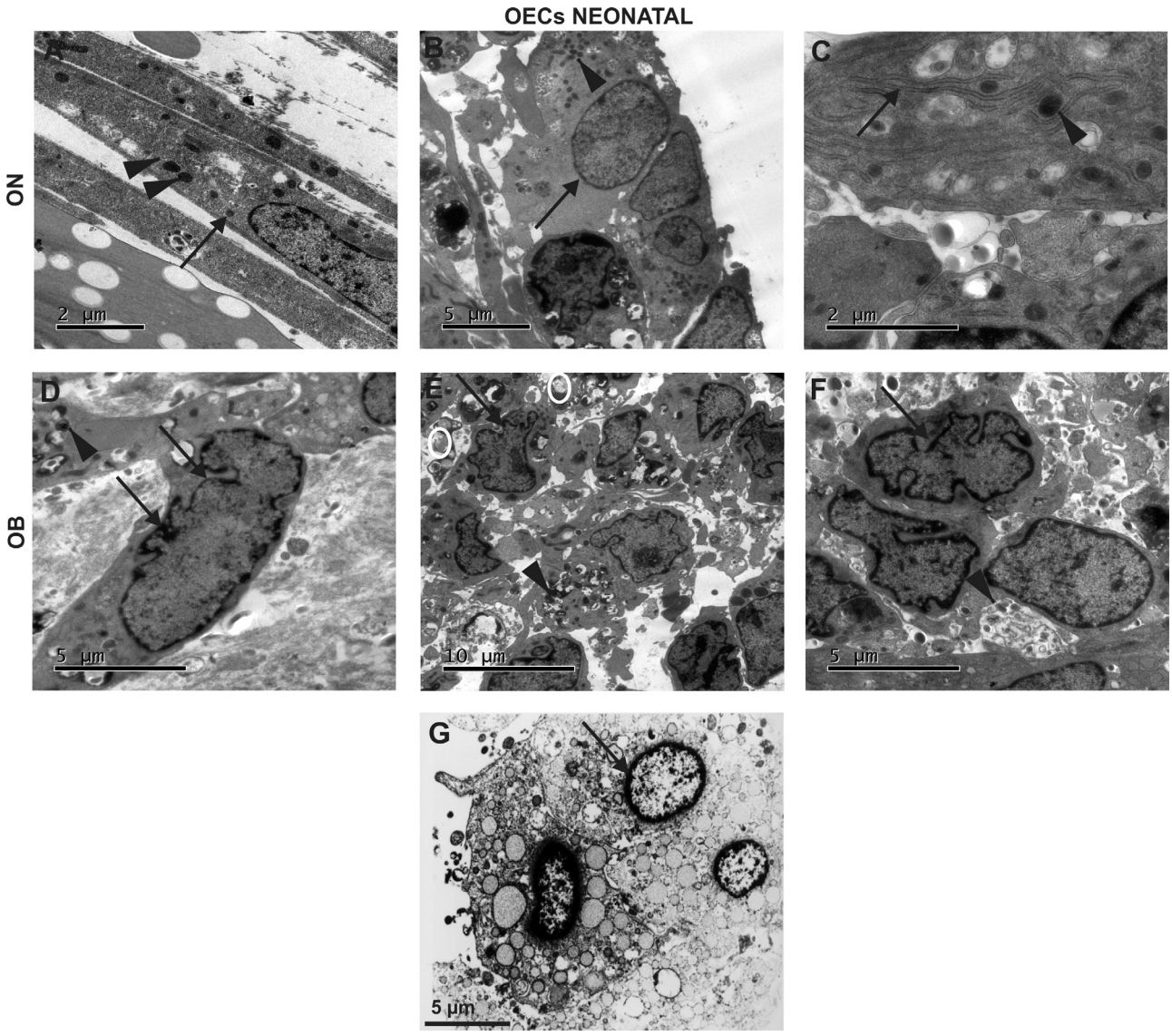


Fig. 5. Microphotograph of neonatal OECs by TEM, labeled with S100B and GFAP. (A–C): Neonatal ON-derived cells. (A) Elongated cells with extended nuclei, some mitochondria (arrow) and lysosomes (arrowheads). (B) Rounded indented nuclei (arrows), presence of abundant mitochondria (arrowheads). (C) Prominent endoplasmic reticulum (arrows) and mitochondria (arrowheads). (D–F): Neonatal OB-derived cells. (D) Extended indented nuclei (arrows), condensed chromatin below the nuclear membrane (arrowhead). (E) Indented nuclei (arrows), mitochondria (arrowheads) and lysosomes (circle). Arrow inset detail of indented nuclei. (F) Prominent endoplasmic reticulum (arrows) and mitochondria (arrowheads).

Table 1
The ultrastructure properties of the OEC in vitro.

	Neonatal	Juvenile
OB	• Have both a spindle and a flattened morphology. • The presence of nuclei rounded but in this case indeed. • In neonatal OECs abundant mitochondria, lipid vacuoles with large size, and smooth endoplasmic reticulum. • Have microscopic properties that could make them more suitable for cell transplantation • Cells spindle-shaped like with large cytoplasm, with a tendency to have a patchy growth pattern with a thick internal membrane • Their shape varied from bipolar spindly to stellate • Presence of phagolysosomes but in less proportion than in juvenile cells	• Have both a spindle and a flattened morphology • The presence of indented and large nuclei with electro dense vacuoles and granules • Nuclei rounded with a nucleus cytoplasm ratio 2:1, with aggregates of heterochromatin at the periphery • Have microscopic properties that could make them more suitable for cell transplantation • Cells spindle-shaped like with large cytoplasm, with a tendency to have a patchy growth pattern with a thick internal membrane • Cells with irregularly shaped • Cells with endoplasmic reticulum • Vesicles with large sized, fragmented and diffuse content (phagolysosomes)
ON	• Have both a spindle and a flattened morphology • Similar to Juvenile cells but with more projections and a nucleus-cytoplasm ratio of 1.5:1. • Nucleus are rounded or elongated, non-indented with peripheral aggregates of heterochromatin • Some cells with a rough endoplasmic reticulum and some mitochondria	• Have both a spindle and a flattened morphology • Their shape varied from bipolar spindly to stellate • Cells with irregularly shaped • Range size from 5 to 20 μm • Polyhedral appearance with cytoplasmic projections, similar to astrocyte cells • Nuclei localized toward one of the ends with a ratio with the cytoplasm of 2.5:1 • The cellular content electro lucid with fiber-shaped structures • The nuclei round or elongated without indentations, with peripheral aggregates of heterochromatin

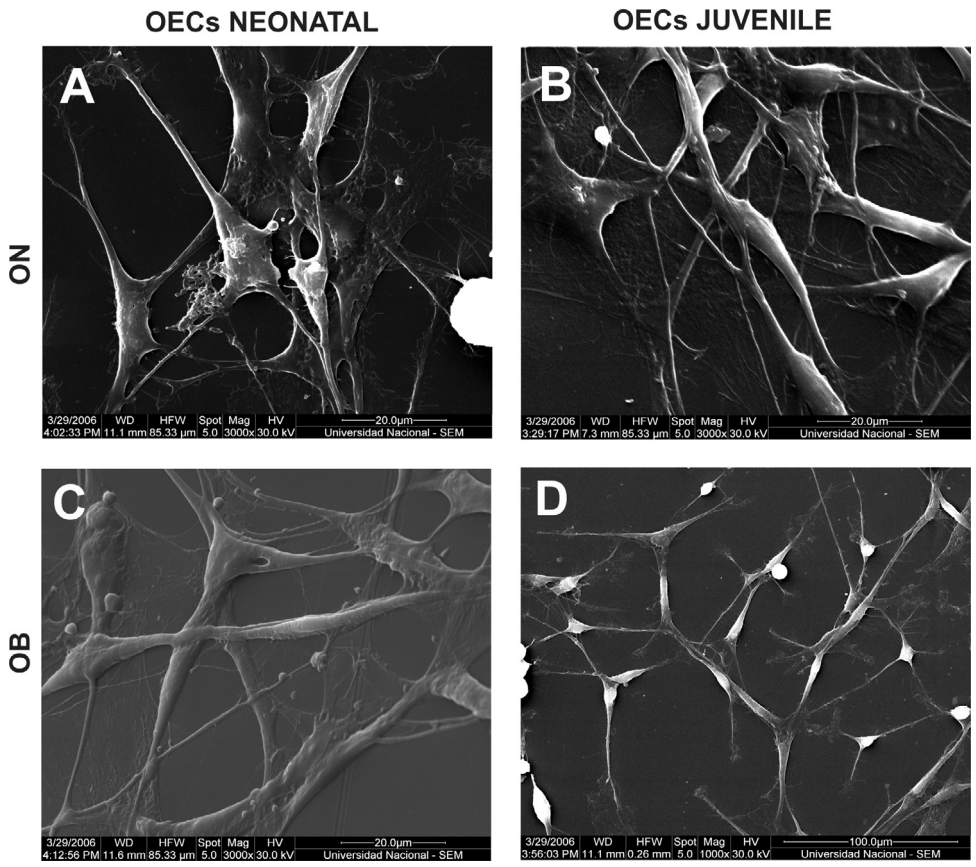


Fig. 6. SEM. (A) Neonatal, ON-derived OECs, (B) Juvenile, ON-derived OECs, (C) Neonatal, OB-derived OECs, (D) Juvenile, OB-derived OECS. Stellate spindle cells are observed, without significant differences regarding morphology in SEM.

findings suggest that neonatal OECs might have an increased ability as myelin-forming cells compared to juvenile OECs, making them more suitable for cell therapy in treatment of SCI and neurodegenerative diseases (Coutts et al., 2013; Kumar et al., 2005; Roet and Verhaagen, 2014; Sasaki et al., 2011). In addition, both cell types (neonatal and juvenile) presented large sized vesicles with fragmented and diffuse content, suggesting an increased phagocytic activity, more prominent in juvenile OECs. Phagocytic function in OECs was recently reported (He et al., 2014), with demonstration of engulfment of degenerated neuron debris, as a substantial contribution to neuron growth.

In summary, results from this study suggest that OB-derived neonatal OECs may be more suitable for cell transplants in SCI models compared to ON-derived and juvenile OECs, based on their microscopic morphological characteristics, indicating possible cell mobility through chemotaxis and lipid metabolic activity related to myelin formation, respectively. However, our study mainly focused on morphological features of OECs, which addressed functional characteristics that are also essential to complement the decision-making process when planning a successful cell transplant. Additional microscopic, morphological and quatitative studies are needed to characterize OECs derived from olfactory lamina (OL) whose retrieval might be technically easier, with potential applications for translational research in clinical trials involving patients with neural repair.

Acknowledgements

The authors appreciate the cooperation extended by the Biological Reagents Laboratory, Institute of Biotechnology, Universidad Nacional de Colombia, and the Special Endowment Fund of the Universidad de La Sabana (Grant MED29).

References

Au, E., Roskams, A.J., 2003. Olfactory ensheathing cells of the lamina propria in vivo and in vitro. Glia 41, 224–236.
Barber, P.C., Lindsay, R.M., 1982. Schwann cells of the olfactory nerves contain glial fibrillary acidic protein and resemble astrocytes. Neuroscience 7, 3077–3090.
Boyd, J.G., Doucette, R., Kawaja, M.D., 2005. Defining the role of olfactory ensheathing cells in facilitating axon remyelination following damage to the spinal cord. FASEB J. 19, 694–703.
Chou, R.H., Lu, C.Y., Wei, L., Fan, J.R., Yu, Y.L., Shyu, W.C., 2014. The potential therapeutic applications of olfactory ensheathing cells in regenerative medicine. Cell Transplant. 23, 567–571.
Coutts, D.J., Humphries, C.E., Zhao, C., Plant, G.W., Franklin, R.J., 2013. Embryonic-derived olfactory ensheathing cells remyelinate focal areas of spinal cord demyelination more efficiently than neonatal or adult-derived cells. Cell Transplant. 22, 1249–1261.
Devon, R., Doucette, R., 1995. Olfactory ensheathing cells do not require L-ascorbic acid in vitro to assemble a basal lamina or to myelinate dorsal root ganglion neurites. Brain Res. 688, 223–229.
Doucette, J.R., 1984. The glial cells in the nerve fiber layer of the rat olfactory bulb. Anat. Rec. 210, 385–391.
Franssen, E.H., de Bree, F.M., Verhaagen, J., 2007. Olfactory ensheathing glia: their contribution to primary olfactory nervous system regeneration and their regenerative potential following transplantation into the injured spinal cord. Brain Res. Rev. 56, 236–258.
Goodman, M.N., Silver, J., Jacobberger, J.W., 1993. Establishment and neurite outgrowth properties of neonatal and adult rat olfactory bulb glial cell lines. Brain Res. 619, 199–213.
He, B.R., Xie, S.T., Wu, M.M., Hao, D.J., Yang, H., 2014. Phagocytic removal of neuronal debris by olfactory ensheathing cells enhances neuronal survival and neurite outgrowth via p38MAPK activity. Mol. Neurobiol. 49, 1501–1512.
Higginson, J.R., Barnett, S.C., 2011. The culture of olfactory ensheathing cells (OECs) – a distinct glial cell type. Exp. Neurol. 229, 2–9.
Hoffmann, K., Sperling, K., Olins, A.L., Olins, D.E., 2007. The granulocyte nucleus and lamin B receptor: avoiding the ovoid. Chromosoma 116, 227–235.

Kocsis, J.D., Lankford, K.L., Sasaki, M., Radtke, C., 2009. Unique in vivo properties of olfactory ensheathing cells that may contribute to neural repair and protection following spinal cord injury. Neurosci. Lett. 456, 137–142.
Kueh, J.L., Raisman, G., Li, Y., Stevens, R., Li, D., 2011. Comparison of bulbar and mucosal olfactory ensheathing cells using FACS and simultaneous antigenic bivariate cell cycle analysis. Glia 59, 1658–1671.
Kumar, R., Hayat, S., Felts, P., Bunting, S., Wigley, C., 2005. Functional differences and interactions between phenotypic subpopulations of olfactory ensheathing cells in promoting CNS axonal regeneration. Glia 50, 12–20.
Leaver, S.G., Harvey, A.R., Plant, G.W., 2006. Adult olfactory ensheathing glia promote the long-distance growth of adult retinal ganglion cell neurites in vitro. Glia 53, 467–476.
Nash, H.H., Borke, R.C., Anders, J.J., 2001. New method of purification for establishing primary cultures of ensheathing cells from the adult olfactory bulb. Glia 34, 81–87.
Ozdemir, M., Attar, A., Kuzu, I., 2012. Regenerative treatment in spinal cord injury. Curr. Stem Cell Res. Ther. 7, 364–369.
Pellitteri, R., Spatuzza, M., Russo, A., Stanzani, S., 2007. Olfactory ensheathing cells exert a trophic effect on the hypothalamic neurons in vitro. Neurosci. Lett. 417, 24–29.
Pellitteri, R., Spatuzza, M., Stanzani, S., Zaccheo, D., 2010. Biomarkers expression in rat olfactory ensheathing cells. Front. Biosci. 2, 289–298.
Pixley, S.K., 1992. The olfactory nerve contains two populations of glia, identified both in vivo and in vitro. Glia 5, 269–284.
Plant, G.W., Harvey, A.R., Leaver, S.G., Lee, S.V., 2011. Olfactory ensheathing glia: repairing injury to the mammalian visual system. Exp. Neurol. 229, 99–108.
Radtke, C., Sasaki, M., Lankford, K.L., Gallo, V., Kocsis, J.D., 2011. CNPase expression in olfactory ensheathing cells. J. Biomed. Biotechnol. 2011, 608496.
Ramon-Cueto, A., Nieto-Sampedro, M., 1992. Glial cells from adult rat olfactory bulb: immunocytochemical properties of pure cultures of ensheathing cells. Neuroscience 47, 213–220.
Ramon-Cueto, A., Perez, J., Nieto-Sampedro, M., 1993. In vitro enfolding of olfactory neurites by p75 NGF receptor positive ensheathing cells from adult rat olfactory bulb. Eur. J. Neurosci. 5, 1172–1180.
Richter, M., Westendorf, K., Roskams, A.J., 2008. Culturing olfactory ensheathing cells from the mouse olfactory epithelium. Methods Mol. Biol. 438, 95–102.
Roet, K.C., Verhaagen, J., 2014. Understanding the neural repair-promoting properties of olfactory ensheathing cells. Exp. Neurol. 261, 594–609.
Sasaki, M., Lankford, K.L., Radtke, C., Honmou, O., Kocsis, J.D., 2011. Remyelination after olfactory ensheathing cell transplantation into diverse demyelinating environments. Exp. Neurol. 229, 88–98.
Sasaki, M., Li, B., Lankford, K.L., Radtke, C., Kocsis, J.D., 2007. Remyelination of the injured spinal cord. Prog. Brain Res. 161, 419–433.
Valverde, F., Santacana, M., Heredia, M., 1992. Formation of an olfactory glomerulus: morphological aspects of development and organization. Neuroscience 49, 255–275.
van den Pol, A.N., Santarelli, J.G., 2003. Olfactory ensheathing cells: time lapse imaging of cellular interactions, axonal support, rapid morphologic shifts, and mitosis. J. Comp. Neurol. 458, 175–194.
Watanabe, K., Kondo, K., Takeuchi, N., Nibu, K., Kaga, K., 2006. Age-related changes in cell density and the proliferation rate of olfactory ensheathing cells in the lamina propria of postnatal mouse olfactory mucosa. Brain Res. 1116, 82–92.
Wewetzer, K., Kern, N., Ebel, C., Radtke, C., Brandes, G., 2005. Phagocytosis of O4+ axonal fragments in vitro by p75− neonatal rat olfactory ensheathing cells. Glia 49, 577–587.
Zhu, Y., Cao, L., Su, Z., Mu, L., Yuan, Y., Gao, L., Qiu, Y., He, C., 2010. Olfactory ensheathing cells: attractant of neural progenitor migration to olfactory bulb. Glia 58, 716–729.